Zheng et al. *Zool. Res.* 2023, 44(6): 993−1002
https://doi.org/10.24272/j.issn.2095-8137.2022.495

ZR | Zoological Research

Article Open Access

Multiplex gene editing reduces oxalate production in primary hyperoxaluria type 1

Rui Zheng[1,#], De-Xin Zhang[1,#], Yan-Jiao Shao[1,#], Xiao-Liang Fang[1], Lei Yang[2], Ya-Nan Huo[2], Da-Li Li[2,*], Hong-Quan Geng[3,*]

[1] *Department of Pediatric Urology*, *Xinhua Hospital Affiliated to Shanghai Jiao Tong University School of Medicine*, *Shanghai* 200092, *China*

[2] *Shanghai Key Laboratory of Regulatory Biology*, *Institute of Biomedical Sciences and School of Life Sciences*, *East China Normal University*, *Shanghai* 200241, *China*

[3] *Division of Pediatric Urology*, *Children's Hospital of Fudan University*, *Shanghai* 201102, *China*

ABSTRACT

Targeting key enzymes that generate oxalate precursors or substrates is an alternative strategy to eliminate primary hyperoxaluria type I (PH1), the most common and life-threatening type of primary hyperoxaluria. The compact Clustered Regularly Interspaced Short Palindromic Repeats (CRISPR) from the *Prevotella* and *Francisella 1* (Cpf1) protein simplifies multiplex gene editing and allows for all-in-one adeno-associated virus (AAV) delivery. We hypothesized that the multiplex capabilities of the Cpf1 system could help minimize oxalate formation in PH1 by simultaneously targeting the hepatic hydroxyacid oxidase 1 (*Hao1*) and lactate dehydrogenase A (*Ldha*) genes. Study cohorts included treated PH1 rats ($Agxt^{Q84X}$ rats injected with AAV-AsCpf1 at 7 days of age), phosphate-buffered saline (PBS)-injected PH1 rats, untreated PH1 rats, and age-matched wild-type (WT) rats. The most efficient and specific CRISPR RNA (crRNA) pairs targeting the rat *Hao1* and *Ldha* genes were initially screened *ex vivo*. *In vivo* experiments demonstrated efficient genome editing of the *Hao1* and *Ldha* genes, primarily resulting in small deletions. This resulted in decreased transcription and translational expression of *Hao1* and *Ldha*. Treatment significantly reduced urine oxalate levels, reduced kidney damage, and alleviated nephrocalcinosis in rats with PH1. No liver toxicity, ex-liver genome editing, or obvious off-target effects were detected. We demonstrated the AAV-AsCpf1 system can target multiple genes and rescue the pathogenic phenotype in PH1, serving as a proof-of-concept for the development of multiplex genome editing-based gene therapy.

Keywords: Hyperoxaluria; Genome editing; Lactate dehydrogenase; Hydroxyacid oxidase 1

INTRODUCTION

Primary hyperoxaluria type 1 (PH1) is an autosomal recessive inherited disorder resulting from a deficiency in the alanine glyoxylate aminotransferase (AGT) enzyme encoded by the *AGXT* gene (Danpure et al., 1987; Hopp et al., 2015; Mandrile et al., 2014). Under normal circumstances, AGT detoxifies the oxalate precursor glyoxylate to glycine in the peroxisomes of hepatocytes. *AGXT* deficiency in PH1 results in an overproduction of oxalate in the liver, and excessive accumulation of oxalate in the urine, ultimately leading to progressive chronic kidney disease generally from relapsing urinary stones (Mandrile et al., 2014; Naderi et al., 2015; Salido et al., 2012). PH1 is the most severe and commonly diagnosed subtype of primary hyperoxaluria, with approximately 50% of patients deteriorating into kidney failure and systemic oxalosis by the age of 40. Vitamin B6 (B6), a precursor of the AGT coenzyme pyridoxal 5'-phosphate (PLP), has been used to reduce oxalate excretion in PH1 for over 50 years, but only shows efficacy in about 30% of PH1 patients (Fargue et al., 2013; Hoyer-Kuhn et al., 2014; Toussaint, 1998). At present, the only curative approach is a combined or sequential liver and kidney transplantation (Mandrile et al., 2014; Naderi et al., 2015).

Recent advances in both basic and clinical research related to primary hyperoxaluria have yielded exciting discoveries, including reduction of hepatic oxalate synthesis through substrate reduction therapy (SRT) in the liver (Lai et al., 2018; Martin-Higueras et al., 2016; Zabaleta et al., 2018; Zheng et al., 2020b), prevention of crystal-induced renal injury (Mulay

Received: 22 March 2023; Accepted: 11 September 2023; Online: 12 September 2023

Foundation items: This work was partially supported by the Science and Technology Commission of Shanghai Municipality (22YF1426900, 20140900200) and National Natural Science Foundation of China (32001057)

[#]Authors contributed equally to this work

*Corresponding authors, E-mail: genghongquan@fudan.edu.cn; dlli@bio.ecnu.edu.cn

et al., 2013, 2016), and reduction in oxalate levels by intestinal elimination (Daniel et al., 2021; Dindo et al., 2019). Among these approaches, SRT has emerged as the most effective for curing PH1, with no observed adverse events. By inhibiting the expression of hepatic glycolate oxidase (GO, encoded by the *HAO1* gene), SRT prevents the conversion of glycolate to glyoxylate, and by inhibiting the expression of hepatic lactate dehydrogenase (LDH, encoded by the *LDHA* gene), SRT further blocks the conversion of glyoxylate to oxalate. Additionally, employing genome editing tools for SRT demonstrates longer-lasting effects than RNA interference (RNAi), which generally requires lifelong repeated dosing. However, the constrained packaging capacity of adeno-associated virus (AAV) vectors and the bulky size of the Cas9 protein have impeded *in vivo* genome editing efficacy and restricted the potential for multiplex gene editing (Hastie & Samulski, 2015; Jinek et al., 2012; Naso et al., 2017; Ran et al., 2015). Therefore, smaller nucleases are of keen interest within the field.

CRISPR from *Prevotella* and *Francisella* 1 (Cpf1) nucleases is an RNA-guided type V class II CRISPR-Cas system (Fonfara et al., 2016; Zetsche et al., 2015). Compared to Cas9, Cpf1 possesses distinct protospacer adjacent motif (PAM) sequences (thymidine-rich DNA sequences) and unique ribonuclease activity that enables the self-processing of crRNA maturation from the pre-crRNA array (Zetsche et al., 2017). This mechanism allows for the potential targeting of multiple genes simultaneously with a single crRNA array. Additional characteristics of Cpf1 include its compact size, self-processing short-length crRNAs, and high specificity for genome-wide targeting, providing a solid basis for translational applications. Nevertheless, to the best of our knowledge, the multiplex genome editing capability of Cpf1 has not yet been applied in any therapeutic evaluation studies.

In this study, we utilized the previously described *Agxt*^{Q84} PH1 rat model (Li et al., 2021) to demonstrate the effectiveness of the Cpf1 system for multiplex gene editing in a real genetic disease scenario. Specifically, we packaged the Cpf1 system targeting hepatic *Hao1* and *Ldha* genes into a single AAV vector. Results showed that this treatment effectively reduced oxalate production and prevented PH1 development, representing the first successful application of the Cpf1 system in a genetic disease model. Overall, our findings provide further evidence of the potential utility of the Cpf1 system in gene therapy and highlight its promising application for the treatment of genetic diseases.

MATERIALS AND METHODS

Plasmid construction

The reporter plasmid used for crRNA *in vitro* screening was constructed by inserting DNA fragments of the codon-optimized open reading frame of AsCpf1 (*Acidaminococcus sp.* Cpf1) (Addgene, plasmid 79007; a gift from Jin-Soo Kim) and U6 promoter-driven direct repeat sequences into a modified pcDNA3.1 vector containing an enhanced green fluorescent protein (EGFP) cassette under the regulation of the elongation factor 1 alpha (EF-1α) promoter. An AAV vector was subsequently generated, cloning AsCpf1 and the CRISPR-Cpf1 array together. DNA fragments of AsCpf1 and the U6 promoter-driven Cpf1 array corresponding to spacer sequences of the rat *Hao1* and *Ldha* genes were cloned into the AAV backbone under the control of a minimized cytomegalovirus (CMV) promoter. All plasmids were generated by standard molecular cloning and assembly.

Cell culture and *in vitro* testing of Cpf1 system

The rat PC12 cell line was purchased from the American Type Culture Collection (ATCC, USA), cultured in Dulbecco's Modified Eagle Medium (DMEM) supplemented with 10% fetal bovine serum (FBS, Gibco, China), and incubated at 37 ℃ in a 5% CO_2 atmosphere. Cells were seeded in 12-well plates, and each well was transfected at 80% confluence with 1.6 μg of reporter plasmids using 4.8 μL of polyethyleneimine (PEI) (Polysciences, China). Cells were transfected for 60 h before DNA extraction and next-generation sequencing (NGS) analysis. All crRNA sequences and primers are listed in Supplementary Table S1.

Animals

Sprague Dawley rats were purchased from the Laboratory Animal Center (Shanghai, China) as wild-type (WT) controls. Rats homozygous for the *Agxt*-Q84X mutation, genotyped as described previously (Li et al., 2021), were generated by breeding homozygous males and females. All animals were housed in clean cages under controlled temperature (22–25 °C), humidity (40%–60%), and light conditions (12 h: 12 h light/dark cycle), with free access to water and food. All animal experiments conformed to the guidelines of the Association for Assessment and Accreditation of Laboratory Animal Care in Shanghai and were approved by the Institutional Animal Care and Use Committee of the Ethics Committee of the Shanghai Jiao Tong University School of Medicine (approval No.: XHEC-STCSM-2022-010). Animal tissue collection is described in the Supplementary Methods.

At week 6 after AAV or phosphate-buffered saline (PBS) injection, a small liver tissue biopsy (median lobe) was collected from each rat under isoflurane anesthesia for genome, mRNA, and protein extraction and histological analysis. At weeks 6 and 24 after AAV or PBS injection, blood was drawn from the retro-orbital venous plexus of the rats for quantification of serum alanine aminotransferase (ALT), aspartate aminotransferase (AST), and total bilirubin (T-BIL) by Servicebio (China).

Urine samples (24 h) were collected from rats in metabolic cages at 6, 14, and 24 weeks after treatment, respectively. Starting at 24 weeks post-treatment, three rats in each group were administered 1% ethylene glycol (EG), which acts as a precursor of glyoxylate and enhances oxalate production (Li et al., 2021), for 2 weeks before sacrifice. Urine samples were collected over 24 h on days 7 and 14 of EG challenge. All animals were then sacrificed by CO_2 inhalation. The left kidney of each rat was weighed and then fixed in 4% paraformaldehyde solution for paraffin sectioning. Skeletal muscle, left ventricle, kidney, spleen, and testis were all harvested for DNA extraction and NGS analysis.

AAV production

AAV-AsCpf1 production, purification, and titer assays were performed as reported previously (Zheng et al., 2020a, 2020b).

Genome editing quantification and gene expression detection

To amplify the genomic region of interest, polymerase chain reaction (PCR) primers with overlapping sequences were designed around on- and off-target sites (Supplementary Table S1) for the quantification of genome editing.

Subsequent PCR was performed by CSGENE (China) using the Illumina HiSeq platform (Illumina, USA). Indel percentage was defined as the number of sequence reads containing insertions and deletions by total number of sequence reads, after excluding background noise.

For *Hao1* and *Ldha* mRNA detection, total RNA was extracted from liver tissue samples using RNAiso Plus (TaKaRa, Japan). For cDNA synthesis, the purified RNA (1 μg) was used in conjunction with PrimeScript^{RT} Master Mix (TaKaRa, Japan) and diluted 1:20 (volume ratio) for quantitative real-time PCR (qRT-PCR). The QuantStudio3 real-time PCR system (Applied Biosystems, USA) was used for qRT-PCR with the primers listed in Supplementary Table S1.

For GO and LDH protein detection, whole livers were sonicated and lysed in ice-cold radioimmunoprecipitation assay (RIPA) buffer supplemented with protease inhibitors (Roche, Germany). A bicinchoninic acid (BCA) protein assay kit (Thermo Fisher Scientific, USA) was used to quantify the protein concentration, and 20 μg of each sample was loaded onto 10% gels for sodium dodecyl sulphate polyacrylamide gel electrophoresis (SDS-PAGE) and nitrocellulose blotting membrane transfer. Bands were detected with anti-GO (Arigo, China), anti-LDH (Abcam, UK), and anti-β-actin antibodies (Sigma, Germany). Blots were imaged with the LI-COR Odyssey® CLx system (LI-COR, USA).

Urinary system evaluation

Metabolic cages were used for urine collection over 24 h, followed by manual measurement of urine volume. Urine samples were acidified with hydrochloric acid to pH<2 to solubilize calcium oxalate (CaOx) crystals before storage at −80 °C. Subsequently, thawed urine samples were pipetted up and down, diluted to 10-fold dilution, and filtered using a 0.22 μm aqueous polyethersulfone needle filter (Anpel, China). Finally, quantitative analysis of urinary oxalate levels was performed by the Instrumental Analysis Center of Shanghai Jiao Tong University using ion-exchange chromatography (Dionex ICS-5000, Thermo Fisher Scientific, USA). Renal CaOx crystals formed following 2 weeks of 1% EG administration were identified using Pizzolato staining (Pizzolato, 1964).

Hematoxylin-eosin (H&E) staining

Liver specimens were stained with H&E. Briefly, liver samples were fixed in a 4% formaldehyde solution for 24 h at 4 °C. The tissue specimens were then dehydrated with a graded ethanol series, embedded in paraffin, cut into sections (4 μm), and stained according to the standard procedures for histomorphological analysis.

Statistical analysis

Data analyses were conducted using GraphPad Prism v8 and Adobe Illustrator 2020 v24.0.1. Results are described as the mean±standard deviation (*SD*) of at least three independent measurements for all experiments. Data were analyzed using two-tailed Student's *t*-test, with significance set as follows: *: P<0.05, **: P<0.01, ***: P<0.001, and ****: P<0.0001.

RESULTS

Selection of efficient and specific crRNA pairs combined with Cpf1

As one of the most efficient Cpf1 orthologs, AsCpf1 can recognize T-rich PAM (TTTN) and has lower off-target effects compared to Cas9 nucleases (Kim et al., 2016). According to the specificity scores predicted by the Benchling platform, crRNAs targeting the rat *Hao1* and *Ldha* genes were designed. The editing efficiency of AsCpf1 combined with the crRNA pairs was evaluated in the PC12 rat cells transfected with the AsCpf1-crRNA plasmid. Results showed that the combination of AsCpf1 and *Hao1*-8 crRNA exerted the highest mutation rate on the *Hao1* gene among the eight predicted crRNAs (Figure 1A). Similarly, *Ldha*-1 crRNA was the most efficient crRNA among the eight *Ldha* candidates (Figure 1B). Hence, *Hao1*-8 and *Ldha*-1 crRNAs (Figure 1C) were selected for subsequent *in vivo* study.

All-in-one AAV-AsCpf1 plasmid construction and validation

The compact size of the AsCpf1 nuclease and simplicity of Cpf1 crRNA maturation allow *in vivo* delivery using an all-in-one AAV serotype 8 vector. We first cloned a minimized CMV-driven AsCpf1 expression cassette along with a U6-driven CRISPR pre-crRNA array into an AAV backbone plasmid (Figure 1D). Two spacers (20 nt) separated by direct repetitions from the AsCpf1 CRISPR locus constituted the CRISPR pre-crRNA array. Subsequently, we examined indel events in the *Hao1*- and *Ldha*-targeted loci in the PC12 cells transfected with the AAV-AsCpf1 plasmid. The indel frequencies in the crRNAs targeting *Hao1* and *Ldha* were 49.7% and 31.7%, respectively, thus confirming the multiplex genome editing ability of the plasmid (Supplementary Figure S1).

AAV-AsCpf1-mediated hepatic *Hao1* and *Ldha* gene mutants

The *Agxt*^{Q84X} PH1 rats (Li et al., 2021) used in this study were divided into three groups: i.e., AAV-treated, untreated, and PBS-injected groups. Age-matched WT rats were used as the control. AAV was diluted in sterile PBS to a final volume of 0.4 mL per rat. In the treatment group, one-week-old *Agxt*^{Q84X} neonatal rats were injected in the tail vein with 5×10^{11} genome copies (GC) of AAV-AsCpf1 targeting *Hao1* and *Ldha*. As single administration of crRNA or CRISPR nucleases can cause rare genome edits (Zabaleta et al., 2018; Zheng et al., 2020b), genome editing efficacy was assessed in the treatment and PBS groups.

Deep sequencing of liver samples revealed robust genome editing in the treatment group, with average indels of 14.1% and 25.1% at the *Hao1* and *Ldha* loci, respectively (Figure 2A). At both target sites, more than 95% of the indels caused by Cpf1 were deletions at the 3' end of the crRNA around the target site (Figure 2B, C; Supplementary Figure S2). This aligns with previous research demonstrating that Cpf1-mediated cleavage generates a staggered cut 5 nt distal from the PAM site (Zetsche et al., 2015), while Cas9 cutting produces a blunt end (Garneau et al., 2010; Gasiunas et al., 2012). The 10 most common deletions detected by NGS are shown in Supplementary Figure S2. The most common mutations observed for the crRNA targets of *Hao1* and *Ldha* were -17 bp and -6 bp deletions, respectively (Figure 2D, E). Specifically, the distribution of deletions varied at different target sites, leading to discrepancies in frameshift mutation frequency (Figure 2D, E). Consistently, Cpf1-mediated cleavage was prone to generate deletions no longer than 30 bp, with a predominance of deletions less than 10 bp (Figure 2F, G).

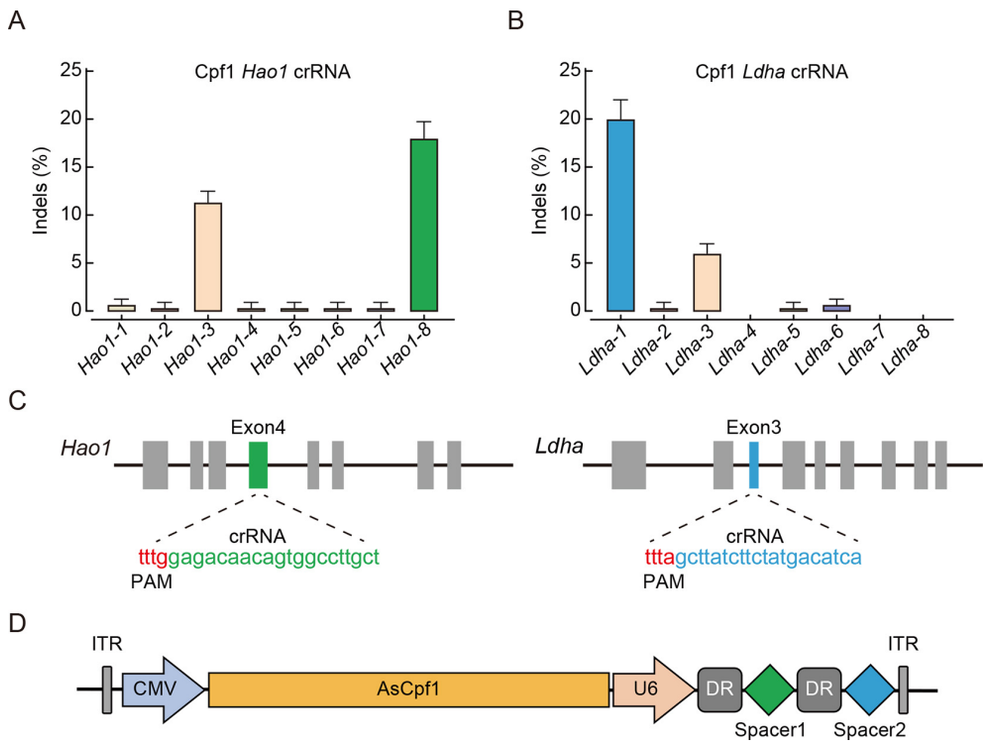

Figure 1 Screening of efficient crRNAs targeting *Hao1* and *Ldha*

A, B: Genome editing efficacy of AsCpf1 across eight endogenous loci within *Hao1* encoding region (A) and *Ldha* encoding region (B). Error bars indicate *SD* (*n*=3). C: Sequences of crRNAs and PAMs are indicated, and crRNA localizations are displayed. D: Schematic representation of all-in-one AAV vector containing AsCpf1 and two crRNAs. DR, direct repetitions; ITR, inverted terminal repeat; CMV, CMV promotor; U6, U6 promotor.

Indels in target genes, especially frameshift mutations, destabilize gene expression. Here, we detected relatively lower *Hao1* and *Ldha* mRNA transcript levels in the AAV-AsCpf1-injected *Agxt*^{Q84X} rats compared to the PBS group (Figure 2H, I). Consistently, western blotting analysis showed that the protein levels of both GO and LDH were markedly reduced in the treatment group (Figure 2J, K).

Therapeutic double gene knockdown ameliorates hyperoxaluria, nephrocalcinosis, and kidney injury

To assess *in vivo* therapeutic efficacy, urine was collected over 24 h to quantify cumulative oxalate excretion. As shown in Figure 3A, the *Agxt*^{Q84X} rats exhibited consistently high urinary oxalate levels, approximately 3.0-fold higher than those of age-matched WT rats. All *Agxt*^{Q84X} rats in the treatment group displayed markedly lower urinary oxalate excretion over the experimental period of 24 weeks. Compared to the untreated group, AAV-AsCpf1 treatment led to mean reductions in urinary oxalate excretion in *Agxt*^{Q84X} rats of 29.5%, 32.8%, and 38.1% at 6, 14, and 24 weeks, respectively.

At 24 weeks post-treatment, both the WT and AAV-AsCpf1-treated *Agxt*^{Q84X} rats exhibited increased urinary oxalate excretion over the EG challenge period (Figure 3B). In the first week of the EG challenge, the PBS-treated *Agxt*^{Q84X} rats showed a pronounced increase in 24 h urinary oxalate levels. In the second week, however, urinary oxalate excretion in the PBS group declined, reaching a comparable level to that observed in the AAV-AsCpf1-treated *Agxt*^{Q84X} rats. This may be attributed to kidney injury, as reflected by elevated serum creatinine levels in the PBS-injected *Agxt*^{Q84X} rats (Figure 3C), suggesting that impaired kidney function resulting from damage may hinder normal oxalate excretion through urine. Accordingly, kidneys from the PBS-treated group displayed a swollen appearance with a significantly elevated weight, approximately 1.7-fold that of the AAV-treated *Agxt*^{Q84} rats and 2.0-fold that of the WT rats (Figure 3D). Similarly, based on terminal deoxynucleotidyl transferase-mediated nick-end labeling (TUNEL) fluorescence analysis (Figure 3E, F), more apoptotic cells were detected in the PBS-injected *Agxt*^{Q84} rats compared to the AAV-treated *Agxt*^{Q84} and WT control rats. Moreover, H&E staining of PBS-injected *Agxt*^{Q84X} rats revealed marked tubular dilation, interstitial fibrosis, extensive areas of tubular atrophy and vacuolization, as well as the presence of numerous calcium oxalate crystals in the tubular lumen (Figure 3G), indicating significant damage to the renal tubular cells. In contrast, AAV-AsCpf1-injected *Agxt*^{Q84X} rats showed only mild tubular dilation and minimal deposition of calcium oxalate crystals.

Pizzolato-stained kidney slices showed distinct differences among the groups (Figure 4). The *Agxt*^{Q84X} rats injected with PBS typically presented with extensive renal CaOx deposits (stained black) along with severely diluted and disrupted tubules in all regions of the kidney (especially the renal cortex). This phenotype was notably ameliorated by AAV-AsCpf1 treatment. Comparatively, all WT kidneys depicted normal morphology.

Toxicity evaluation and off-target effects of AAV-AsCpf1

We first performed histological examination of the rat liver tissues. Based on H&E staining, no abnormalities, such as liver fibrosis and immune cell infiltration, were observed in any group (Figure 5A). Furthermore, biochemical indicators of liver function, such as serum ALT, AST, and T-BIL levels, fluctuated within a small range for all three groups (Figure 5B), suggesting no apparent short- or long-term liver toxicity (6 to 24 weeks). In addition, ex-liver tissues were obtained to test the specificity of AAV-AsCpf1 treatment. Results showed no

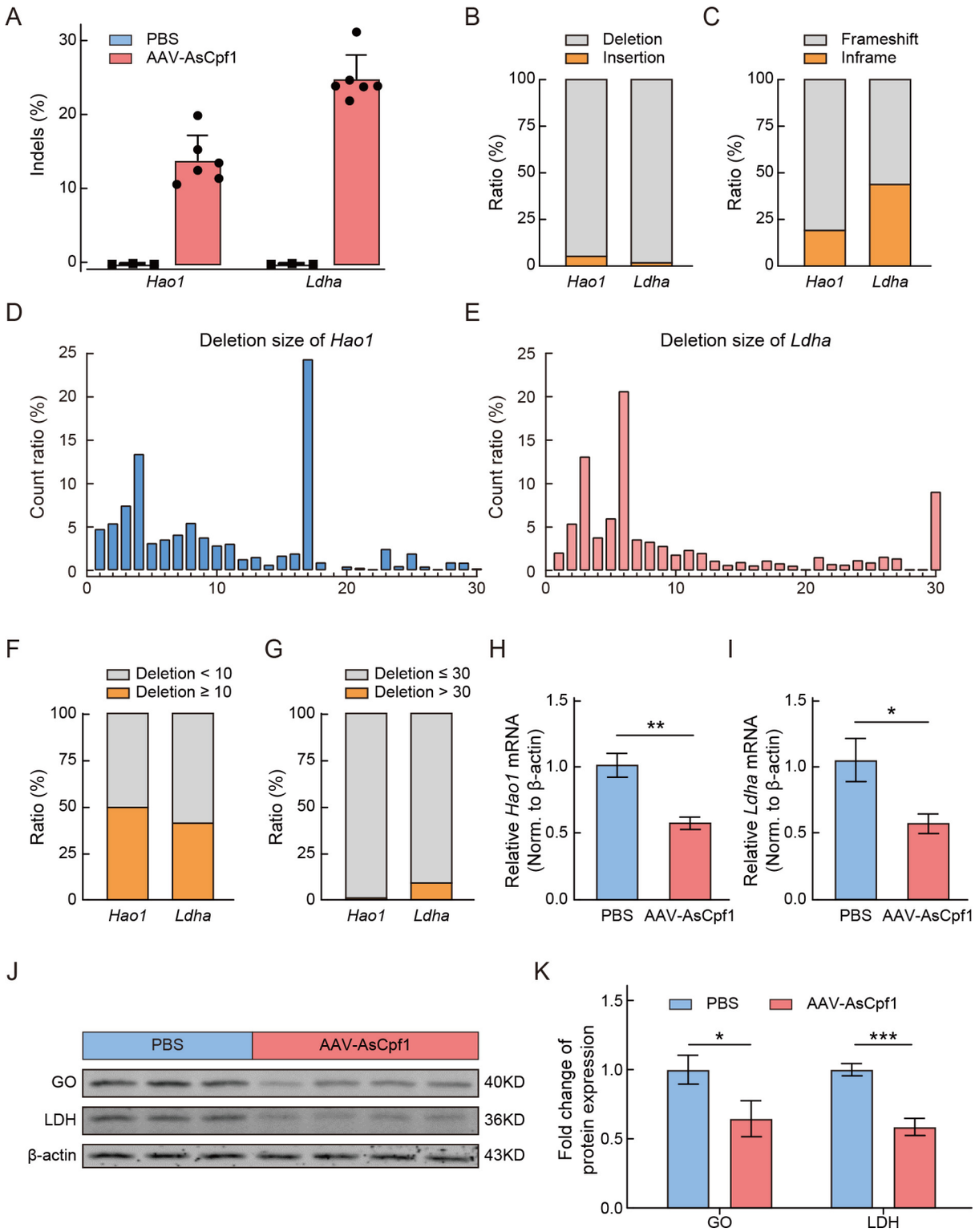

Figure 2 Detection of Cpf1-mediated gene editing

A: *In vivo* indel efficiencies at *Hao1* and *Ldha* loci in PH1 rats treated with PBS (*n*=3) and AAV-AsCpf1 (*n*=6), determined by deep sequencing. B: Proportion of insertions and deletions in *Hao1* and *Ldha* loci induced by Cpf1. C–G: Distribution of types and sizes of deleted nucleotide fragments generated by Cpf1. H, I: mRNA levels of *Hao1* and *Ldha* revealed by RT-qPCR, with gene expression normalized to endogenous β-actin. J: Western blot analysis of GO and LDH protein expression. K: Intensity of each band was quantified and normalized to β-actin. *: P<0.05; **: P<0.01; ***: P<0.001, two-tailed t-test.

evidence of gene editing beyond background levels in the muscle, heart, kidney, and spleen tissues of treated *Agxt*^{Q84X} rats compared to the untreated control (Figure 5C, D). The on-target indel frequencies within the testis tissue and somatic genome of AAV-AsCpf1-injected *Agxt*^{Q84X} rat offspring were both negligible (Figure 5C, D), demonstrating that the treatment did not edit the germline genome.

Off-target cleavage at similar target sites in the host

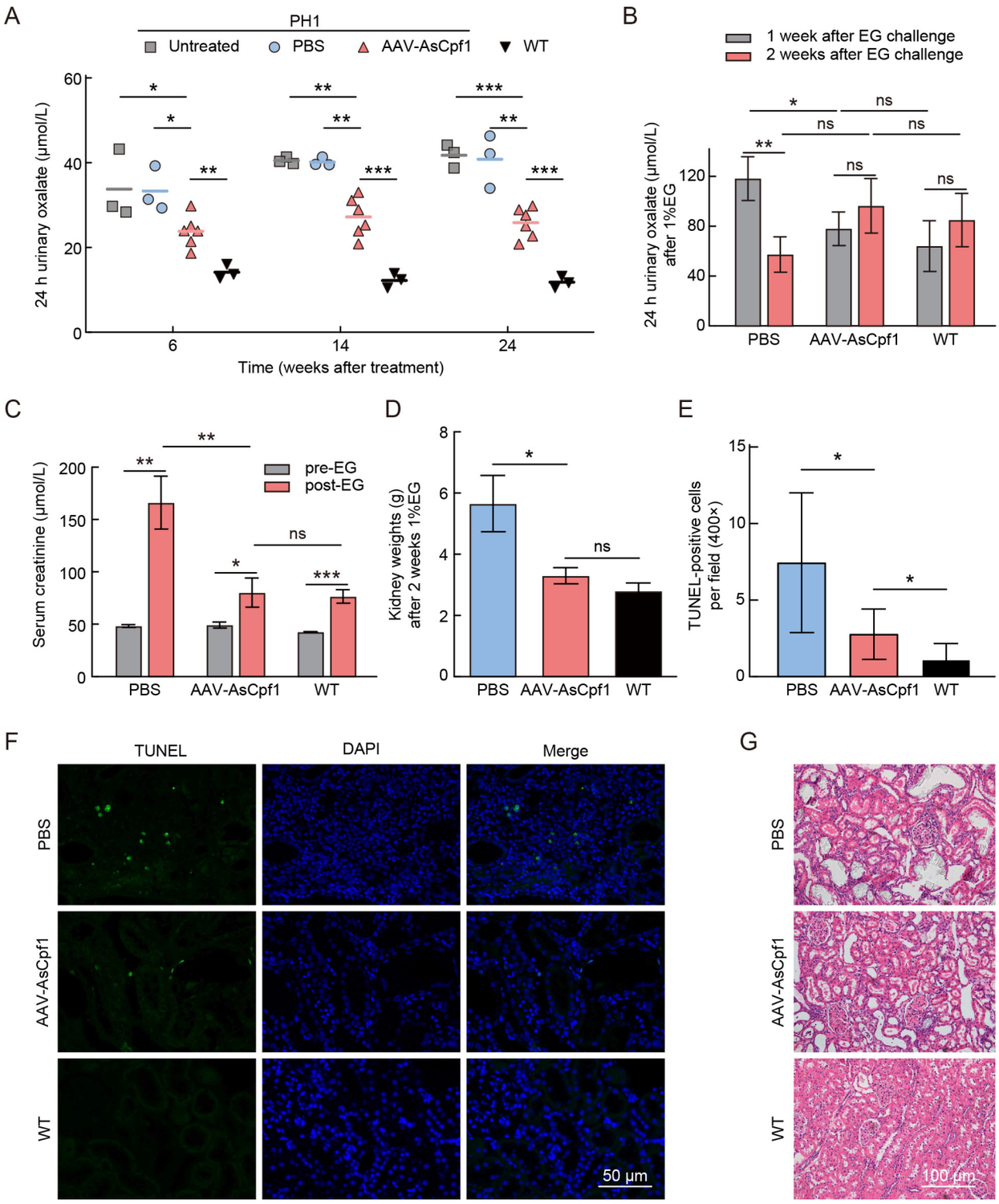

Figure 3 Therapeutic effects of Cpf1-mediated gene therapy

A: Quantification of urinary oxalate levels over 24 h in untreated (*n*=3), PBS-treated (*n*=3), AAV-AsCpf1-treated (*n*=6), and WT rats (*n*=3). B: Urinary oxalate analyses over 24 h in rats receiving 1% EG challenge for one and two weeks (*n*=3 in each group), starting at 24 weeks after treatment. C, D: Analysis of serum creatinine (C) and left kidney weights (D) after 2 weeks of EG feeding. E: Renal cell death was quantified by counting TUNEL-positive cells. For each animal, three random sections were analyzed per field (400×). F: Representative images of TUNEL-stained kidney sections. G: Representative H&E-stained kidney sections. Data represent mean±*SD*. ns: Not significant; *: *P*<0.05; **: *P*<0.01; ***: *P*<0.001, two-tailed *t*-test.

genome is a major concern for genome editing technologies. Therefore, we identified ten potential off-target sites for *Hao1*-crRNA and eight sites for *Ldha*-crRNA with a high risk of genome editing predicted using the Benchling platform. Based on deep sequencing of genomic DNA extracted from total liver cells, indel frequencies were below 1% at most sites for the *Hao1* and *Ldha* targets (Figure 5E, F). The top two off-target sites of *Ldha* crRNA with an indel frequency greater than 1% were located in pseudogenes with no significant known biological function. These results confirm that the combination of crRNA with Cpf1 was highly specific in targeting both *Hao1* and *Ldha*.

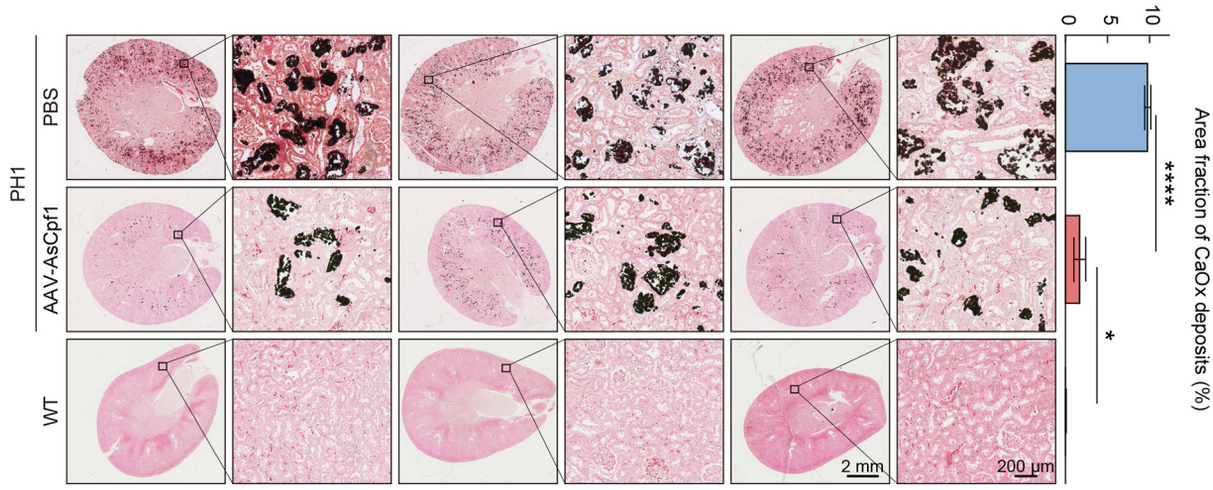

Figure 4 Evaluation of nephrocalcinosis in PH1 and WT rats after EG challenge

(left) Representative histological analysis of renal calcium oxalate (CaOx) precipitation in six-month-old PH1 and WT rats after 2 weeks of EG challenge. (right) Quantification of CaOx areas (%) in renal sections. Scale bar: 2 mm. *: P<0.05; ****: P<0.0001, two-tailed t-test.

DISCUSSION

In this study, we used the multiplex genome editing property of Cpf1 to simultaneously target two genes related to hepatic oxalate synthesis, *Hao1* and *Ldha*, to alleviate PH1. Within the coding regions of *Hao1* and *Ldha*, the most efficient crRNAs with predicted high specificity were designed and validated *in vitro*. Subsequently, we validated the maturation of crRNAs by Cpf1 alone using the all-in-one AAV vector and produced AAV viral particles for *in vivo* administration. Results showed that the treatment reduced urinary oxalate levels, protected kidney function, and minimized renal CaOx deposition in PH1 rats, with no off-target effects in the genome or organs. These findings highlight the potential of Cpf1 as a robust tool for multiplex genome editing gene therapy.

In PH1, the innovative SRT strategy was initially tested using small RNAi (siRNA) to inhibit GO and LDH in the liver (Lai et al., 2018; Liebow et al., 2017; Martin-Higueras et al., 2016; Wood et al., 2019). Following this, two phase III clinical trials of lumasiran (inhibiting GO, NCT03681184, and NCT03905694) and one phase II trial of nedosiran (inhibiting LDH, NCT03847909) provided preliminary evidence supporting the safety and efficacy of this approach in treating pediatric PH1 populations, paving the way for the recent approval of lumasiran in the USA and Europe to treat PH1 at all stages (Shah & Pyle, 2021). Notably, compared to the repetitive administration required for RNAi, SRT combined with gene editing technology can provide long-term benefits for PH1.

This study successfully integrated two crRNAs and miniature Cpf1 nuclease into one AAV vehicle, which simultaneously disrupted 14.1% of *Hao1* and 25.1% of *Ldha* alleles in the whole liver tissue, resulting in a 38.1% reduction in urinary oxalate levels. Similarly, in our previous studies based on single gene targeting, we achieved indel frequencies of 29.4% and 18.6% in *Hao1* and *Ldha*, respectively, leading to a reduction in urinary oxalate levels of 42.0% and 33.6%, respectively (Zheng et al., 2020a, 2020b). In contrast, Zabaleta et al. (2018) reported a remarkable therapeutic effect in PH1 murine models using AAV-mediated CRISPR/Cas9 genome editing to target the *Hao1* gene, achieving a urinary oxalate reduction of nearly 60%, attributed to high gene editing efficiency (approximately 50%) and near-complete suppression of the GO protein. Despite the above, we did not observe an additive effect in this multiplex targeting study. A plausible explanation could be that dual knockout of both genes in an individual cell may not further decrease oxalate levels as *Hao1* and *Ldha* share an oxalate metabolism pathway. In this context, enhancing therapeutic efficacy via multi-gene editing may rely on expanding the population of effectively edited hepatocytes, regardless of whether they have undergone single or double editing. Alternatively, the overlapping therapeutic effects may have been shielded due to suboptimal editing efficiency. A certain editing efficiency threshold is necessary (Lai et al., 2018; Liebow et al., 2017), especially for *Hao1*, to trigger a therapeutic response. Thus, the editing efficiency of Cpf1 requires further optimization. Efforts should be directed towards the development of enhanced Cpf1 variants or identification of Cpf1 variants that recognize PAMs outside the restricted TTTN sequence (Gao et al., 2017), thus expanding the pool of potential crRNA targets with higher efficiency. Enhancing *in vivo* gene editing could also be achieved through the engineering of novel delivery vectors, such as lipid nanoparticles (LNPs), which exhibit strong transduction efficiency and hepatocyte specificity (Finn et al., 2018; Qiu et al., 2021). The large packaging capacity of LNPs enables the integration of multiple elements, such as fluorescent markers, additional crRNAs, and even large-sized base editors (Gaudelli et al., 2017; Komor et al., 2016). Furthermore, the LNP-RNA system allows for relatively precise control over the crRNA and Cpf1 mRNA dosage, which is advantageous for establishing rigorous control groups with single-gene knockout.

Safety and accuracy are essential for the clinical utility of genome editing. AAV vectors are well established in clinical trials for *in vivo* gene therapy due to their broad tropism, low immunogenicity, non-pathogenicity, and durable expression (Hastie & Samulski, 2015; Wu et al., 2006). However, concerns have been raised about their proclivity to generate immune responses to AAV-transduced cells, especially when administered high doses (Hu et al., 2021; Rabinowitz et al., 2019). In the present study, no evidence of hepatic injury or inflammatory cell infiltration was detected under moderate AAV dosing, consistent with previous findings in AAV-treated rats (Naso et al., 2017; Salido et al., 2006; Zabaleta et al., 2018; Zheng et al., 2020a, 2020b). To reveal the full potential

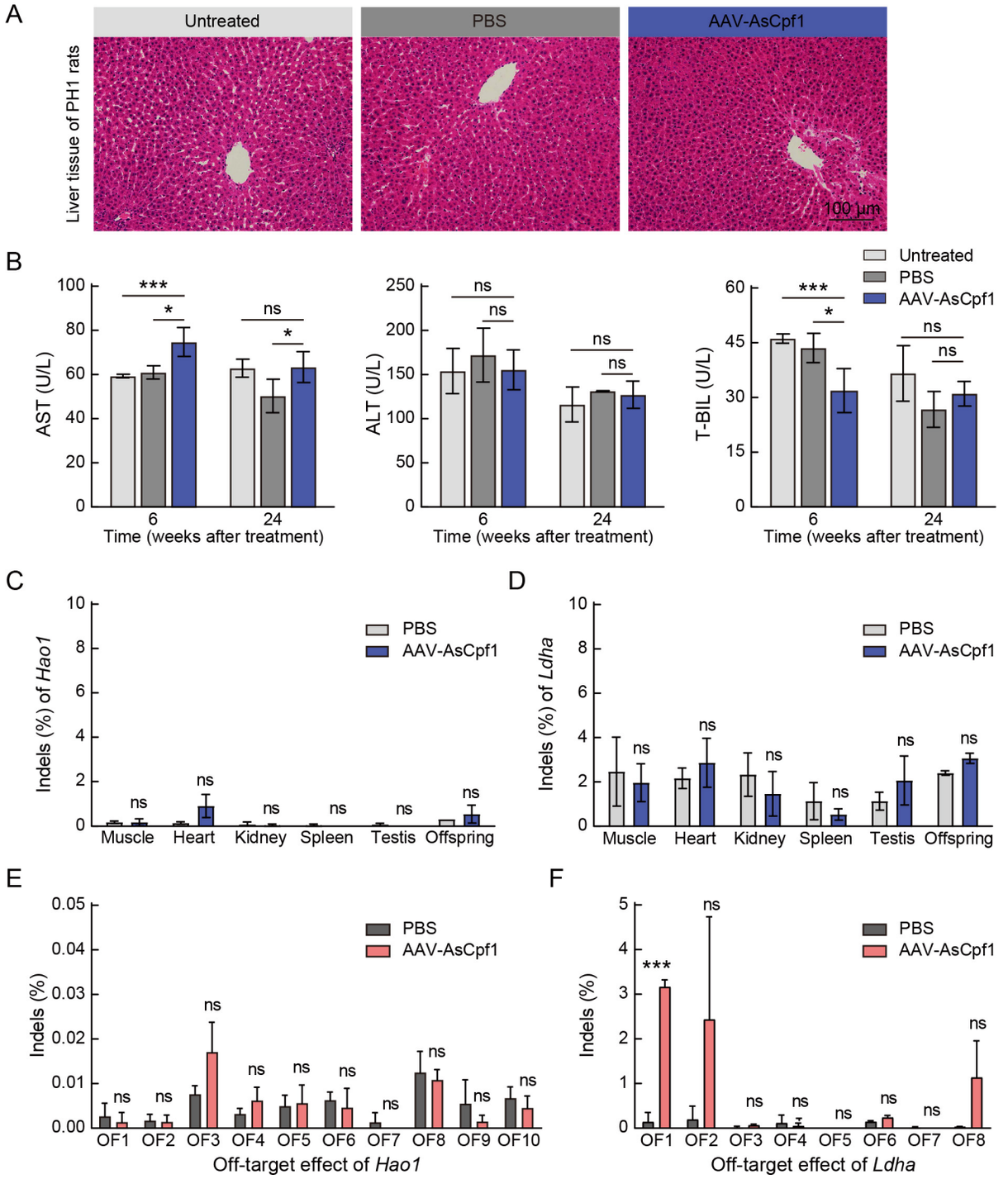

Figure 5 Safety analysis of AAV-AsCpf1-mediated gene therapy

A: Histological analysis of livers by H&E staining. Scale bar, 100 μm. B: Serum AST, ALT, and T-BIL levels (n=3, 3, and 6 in untreated, PBS-treated, and AAV-AsCpf1-treated groups, respectively). C, D: Deep sequencing analysis of *Hao1* and *Ldha* indels in ex-liver organs and AAV-AsCpf1-treated offspring. E, F: Deep sequencing analysis of *Hao1* and *Ldha* crRNA-dependent off-target sites predicted using the Benchling platform. Data represent mean±*SD*. ns: Not significant; *: P<0.05; ***: P<0.001, two-tailed t-test.

of AAV, efforts have been made in viral vector engineering to maximize AAV transduction efficiency and minimize vector dose-dependent immunogenicity (Li & Samulski, 2020; Verdera et al., 2020). However, the potential off-target effects of genome editing have remained a major obstacle to translational application. Here, NGS analysis revealed limited off-target edits in the predicted sites, emphasizing the high specificity of AsCpf1, as demonstrated in previous genome-wide analysis (Kim et al., 2016). Specifically, for *Ldha*-targeting crRNA, limited edits were detected at two predicted off-target sites in pseudogenes showing extensive homology to the rat *Ldha* gene. These findings not only highlight the importance of crRNA design but also suggest that the off-target edits are crRNA sequence-dependent rather than nuclease-relevant. Other factors that may impact the clinical application of genome editing include Cpf1 immunogenicity and the risk associated with pre-existing antibodies against Cpf1, which may lead to unforeseen long-term adverse events

(Chew, 2018).

In conclusion, our study validated the efficacy of Cpf1 for multiplex genome editing *in vivo* using an all-in-one AAV vehicle, resulting in a concomitant decrease in urinary oxalate levels and renal CaOx deposits. With the development of augmented and PAM-modified Cpf1 variants, as well as novel vectors, it is anticipated that the Cpf1 system will expand its utility in both basic research and therapeutic applications in the future.

DATA AVAILABILITY

Raw data were deposited in the National Center for Biotechnology Information database (PRJNA828129), Genome Sequence Archive (PRJCA016479), and Science Data Bank database (DOI: 10.57760/sciencedb.j00139.00052).

SUPPLEMENTARY DATA

Supplementary data to this article can be found online.

COMPETING INTERESTS

The authors declare that they have no competing interests.

AUTHORS' CONTRIBUTIONS

H.Q.G. and D.L.L.: Supervision, Conceptualization, Methodology. R.Z., D.X.Z., and X.L.F.: Data curation, Writing-Original draft preparation. R.Z., Y.J.S., D.X.Z., L.Y., and Y.N.H.: Visualization, Investigation. R.Z.: Software, Validation. H.Q.G.: Writing-Reviewing and Editing. All authors read and approved the final version of the manuscript.

ACKNOWLEDGMENTS

We would like to thank Jing-Yu Zang for figure optimization. We would like to thank CureEdit (www.wscureedit.com) for English language editing of this manuscript.

REFERENCES

Chew WL. 2018. Immunity to CRISPR Cas9 and Cas12a therapeutics. *WIREs Systems Biology and Medicine*, **10**(1): e1408.

Daniel SL, Moradi L, Paiste H, et al. 2021. Forty years of *Oxalobacter formigenes*, a gutsy oxalate-degrading specialist. *Applied and Environmental Microbiology*, **87**(18): e0054421.

Danpure CJ, Jennings PR, Watts RW. 1987. Enzymological diagnosis of primary hyperoxaluria type 1 by measurement of hepatic alanine: glyoxylate aminotransferase activity. *The Lancet*, **1**(8528): 289−291.

Dindo M, Conter C, Oppici E, et al. 2019. Molecular basis of primary hyperoxaluria: clues to innovative treatments. *Urolithiasis*, **47**(1): 67−78.

Fargue S, Rumsby G, Danpure CJ. 2013. Multiple mechanisms of action of pyridoxine in primary hyperoxaluria type 1. *Biochimica et Biophysica Acta (BBA) - Molecular Basis of Disease*, **1832**(10): 1776−1783.

Finn JD, Smith AR, Patel MC, et al. 2018. A single administration of CRISPR/Cas9 lipid nanoparticles achieves robust and persistent *in vivo* genome editing. *Cell Reports*, **22**(9): 2227−2235.

Fonfara I, Richter H, Bratovič M, et al. 2016. The CRISPR-associated DNA-cleaving enzyme Cpf1 also processes precursor CRISPR RNA. *Nature*, **532**(7600): 517−521.

Gao LY, Cox DBT, Yan WX, et al. 2017. Engineered Cpf1 variants with altered PAM specificities. *Nature Biotechnology*, **35**(8): 789−792.

Garneau JE, Dupuis MÈ, Villion M, et al. 2010. The CRISPR/Cas bacterial immune system cleaves bacteriophage and plasmid DNA. *Nature*, **468**(7320): 67−71.

Gasiunas G, Barrangou R, Horvath P, et al. 2012. Cas9-crRNA ribonucleoprotein complex mediates specific DNA cleavage for adaptive immunity in bacteria. *Proceedings of the National Academy of Sciences of the United States of America*, **109**(39): E2579−E2586.

Gaudelli NM, Komor AC, Rees HA, et al. 2017. Programmable base editing of A•T to G•C in genomic DNA without DNA cleavage. *Nature*, **551**(7681): 464−471.

Hastie E, Samulski RJ. 2015. Adeno-associated virus at 50: a golden anniversary of discovery, research, and gene therapy success—a personal perspective. *Human Gene Therapy*, **26**(5): 257−265.

Hopp K, Cogal AG, Bergstralh EJ, et al. 2015. Phenotype-genotype correlations and estimated carrier frequencies of primary hyperoxaluria. *Journal of the American Society of Nephrology*, **26**(10): 2559−2570.

Hoyer-Kuhn H, Kohbrok S, Volland R, et al. 2014. Vitamin B6 in primary hyperoxaluria I: first prospective trial after 40 years of practice. *Clinical Journal of the American Society of Nephrology*, **9**(3): 468−477.

Hu HM, Mosca R, Gomero E, et al. 2021. AAV-mediated gene therapy for galactosialidosis: a long-term safety and efficacy study. *Molecular Therapy - Methods & Clinical Development*, **23**: 644−658.

Jinek M, Chylinski K, Fonfara I, et al. 2012. A programmable dual-RNA-guided DNA endonuclease in adaptive bacterial immunity. *Science*, **337**(6096): 816−821.

Kim D, Kim J, Hur JK, et al. 2016. Genome-wide analysis reveals specificities of Cpf1 endonucleases in human cells. *Nature Biotechnology*, **34**(8): 863−868.

Komor AC, Kim YB, Packer MS, et al. 2016. Programmable editing of a target base in genomic DNA without double-stranded DNA cleavage. *Nature*, **533**(7603): 420−424.

Lai C, Pursell N, Gierut J, et al. 2018. Specific inhibition of hepatic lactate dehydrogenase reduces oxalate production in mouse models of primary hyperoxaluria. *Molecular Therapy*, **26**(8): 1983−1995.

Li CW, Samulski RJ. 2020. Engineering adeno-associated virus vectors for gene therapy. *Nature Reviews Genetics*, **21**(4): 255−272.

Li YY, Zheng R, Xu GF, et al. 2021. Generation and characterization of a novel rat model of primary hyperoxaluria type 1 with a nonsense mutation in alanine-glyoxylate aminotransferase gene. *American Journal of Physiology-Renal Physiology*, **320**(3): F475−F484.

Liebow A, Li XS, Racie T, et al. 2017. An investigational RNAi therapeutic targeting glycolate oxidase reduces oxalate production in models of primary hyperoxaluria. *Journal of the American Society of Nephrology*, **28**(2): 494−503.

Mandrile G, Van Woerden CS, Berchialla P, et al. 2014. Data from a large European study indicate that the outcome of primary hyperoxaluria type 1 correlates with the AGXT mutation type. *Kidney International*, **86**(6): 1197−1204.

Martin-Higueras C, Luis-Lima S, Salido E. 2016. Glycolate oxidase is a safe and efficient target for substrate reduction therapy in a mouse model of primary hyperoxaluria type I. *Molecular Therapy*, **24**(4): 719−725.

Mulay SR, Desai J, Kumar SV, et al. 2016. Cytotoxicity of crystals involves RIPK3-MLKL-mediated necroptosis. *Nature Communications*, **7**: 10274.

Mulay SR, Kulkarni OP, Rupanagudi KV, et al. 2013. Calcium oxalate crystals induce renal inflammation by NLRP3-mediated IL-1β secretion. *Journal of Clinical Investigation*, **123**(1): 236−246.

Naderi G, Tabassomi F, Latif A, et al. 2015. Primary hyperoxaluria type 1 diagnosed after kidney transplantation: the importance of pre-transplantation metabolic screening in recurrent urolithiasis. *Saudi Journal of Kidney Diseases and Transplantation*, **26**(4): 783−785.

Naso MF, Tomkowicz B, Perry III WL, et al. 2017. Adeno-associated virus (AAV) as a vector for gene therapy. *BioDrugs*, **31**(4): 317−334.

Pizzolato P. 1964. Histochemical recognition of calcium oxalate. *Journal of Histochemistry & Cytochemistry*, **12**(5): 333−336.

Qiu M, Glass Z, Chen JJ, et al. 2021. Lipid nanoparticle-mediated codelivery of Cas9 mRNA and single-guide RNA achieves liver-specific in vivo genome editing of *Angptl3*. *Proceedings of the National Academy of Sciences of the United States of America*, **118**(10): e2020401118.

Rabinowitz J, Chan YK, Samulski RJ. 2019. Adeno-associated virus (AAV) versus immune response. *Viruses*, **11**(2): 102.

Ran FA, Cong L, Yan WX, et al. 2015. *In vivo* genome editing using *Staphylococcus aureus* Cas9. *Nature*, **520**(7546): 186−191.

Salido E, Pey AL, Rodriguez R, et al. 2012. Primary hyperoxalurias: disorders of glyoxylate detoxification. *Biochimica et Biophysica Acta (BBA) - Molecular Basis of Disease*, **1822**(9): 1453−1464.

Salido EC, Li XM, Lu Y, et al. 2006. Alanine-glyoxylate aminotransferase-deficient mice, a model for primary hyperoxaluria that responds to adenoviral gene transfer. *Proceedings of the National Academy of Sciences of the United States of America*, **103**(48): 18249−18254.

Shah VN, Pyle L. 2021. Lumasiran, an RNAi therapeutic for primary hyperoxaluria type 1. *The New England Journal of Medicine*, **385**(20): e69.

Toussaint C. 1998. Pyridoxine-responsive PH1: treatment. *Journal of Nephrology*, **11 Suppl 1**: 49–50.

Verdera HC, Kuranda K, Mingozzi F. 2020. AAV vector immunogenicity in humans: a long journey to successful gene transfer. *Molecular Therapy*, **28**(3): 723−746.

Wood KD, Holmes RP, Erbe D, et al. 2019. Reduction in urinary oxalate excretion in mouse models of primary hyperoxaluria by RNA interference inhibition of liver lactate dehydrogenase activity. *Biochimica et Biophysica Acta (BBA) - Molecular Basis of Disease*, **1865**(9): 2203−2209.

Wu ZJ, Asokan A, Samulski RJ. 2006. Adeno-associated virus serotypes: vector toolkit for human gene therapy. *Molecular Therapy*, **14**(3): 316−327.

Zabaleta N, Barberia M, Martin-Higueras C, et al. 2018. CRISPR/Cas9-mediated glycolate oxidase disruption is an efficacious and safe treatment for primary hyperoxaluria type I. *Nature Communications*, **9**(1): 5454.

Zetsche B, Gootenberg JS, Abudayyeh OO, et al. 2015. Cpf1 is a single RNA-guided endonuclease of a class 2 CRISPR-cas system. *Cell*, **163**(3): 759−771.

Zetsche B, Heidenreich M, Mohanraju P, et al. 2017. Multiplex gene editing by CRISPR-Cpf1 using a single crRNA array. *Nature Biotechnology*, **35**(1): 31−34.

Zheng R, Fang XL, Chen X, et al. 2020a. Knockdown of lactate dehydrogenase by adeno-associated virus-delivered CRISPR/Cas9 system alleviates primary hyperoxaluria type 1. *Clinical and Translational Medicine*, **10**(8): e261.

Zheng R, Li YY, Wang LR, et al. 2020b. CRISPR/Cas9-mediated metabolic pathway reprogramming in a novel humanized rat model ameliorates primary hyperoxaluria type 1. *Kidney International*, **98**(4): 947−957.